Supplement of Ocean Sci., 21, 2001–2018, 2025
https://doi.org/10.5194/os-21-2001-2025-supplement

Ocean Science Open Access EGU

Supplement of

The historical representation and near-future (2050) projections of the Coral Sea current system in CMIP6 HighResMIP

Jodie A. Schlaefer et al.

Correspondence to: Jodie A. Schlaefer (jodie.schlaefer@csiro.au)

Supplement

Contents of this file

Table S1

Figures S1 to S17

Table S1. The simulated or observed warming of the global average near-surface air temperature with reference to the pre-industrial 1850 – 1879 historical period as of December 2023, and the simulated years of onset of 1.5°C and 2°C warming. Data sources same as Figure 2.

	Degrees warming at Dec. 2023 (°C)	Year of onset of 1.5°C warming	Year of onset of 2°C warming
CESM	1.84	2015	2027
CMCC	1.59	2020	2037
FGOALS	1.34	2029	2046
SSP5-8.5	1.85	2014	2027
SSP2-4.5	1.56	2021	2041
observed	1.24	NA	NA

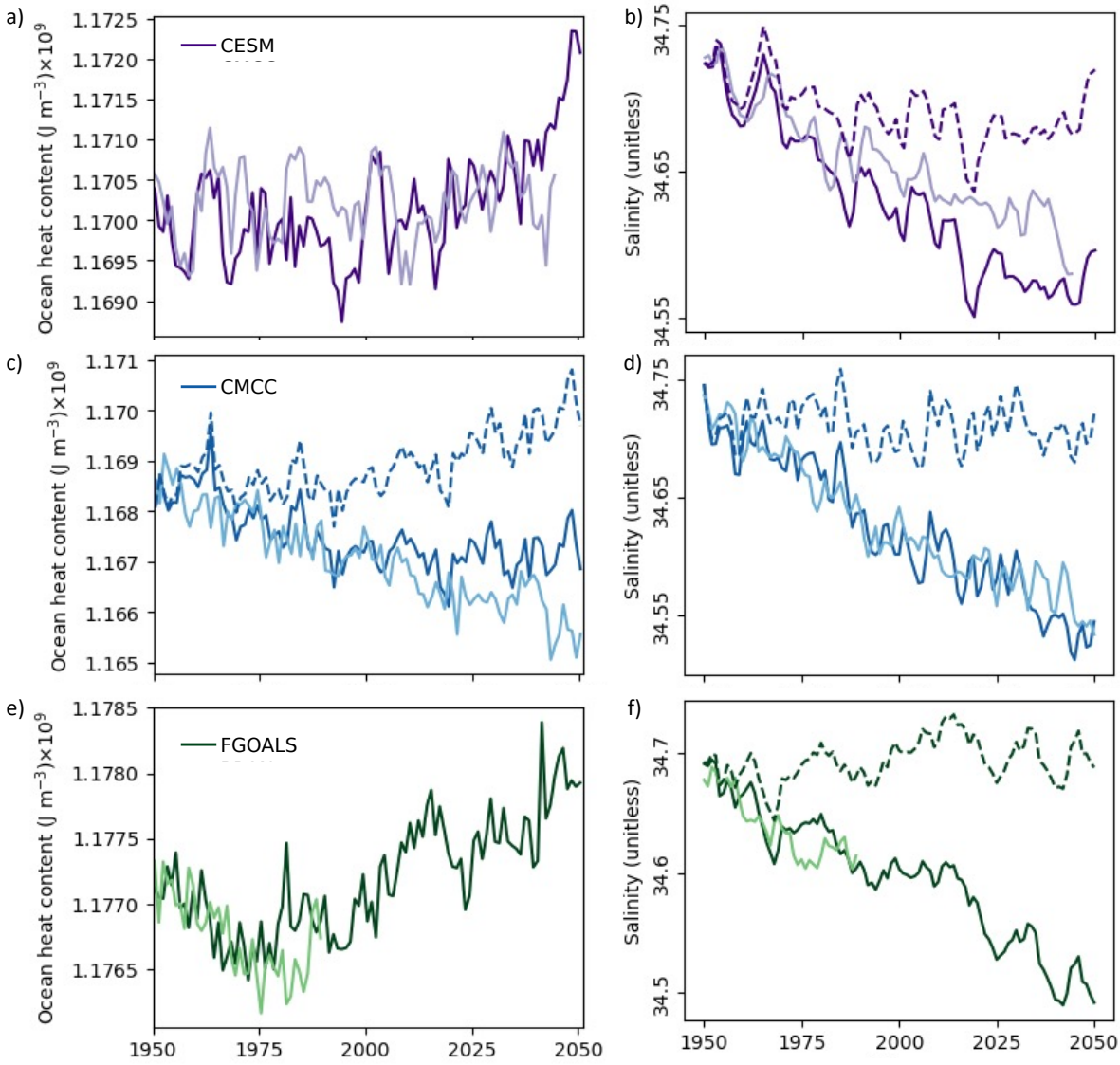

Figure S1. Drift analysis and removal. Change in annual average ocean heat content (left column) and salinity (right column) of the Coral Sea through time in CMIP6 HighResMIP models. a, b) CESM. c, d) CMCC. e, f) FGOALS. Dark solid lines show the SSP5-8.5 simulations. Light solid lines show the control-1950 simulations, with fixed 1950's atmospheric forcings including climatological 1950's greenhouse gas levels. Where applicable, dashed dark lines show the SSP5-8.5 simulations after the removal of the drifts identified from the control simulations.

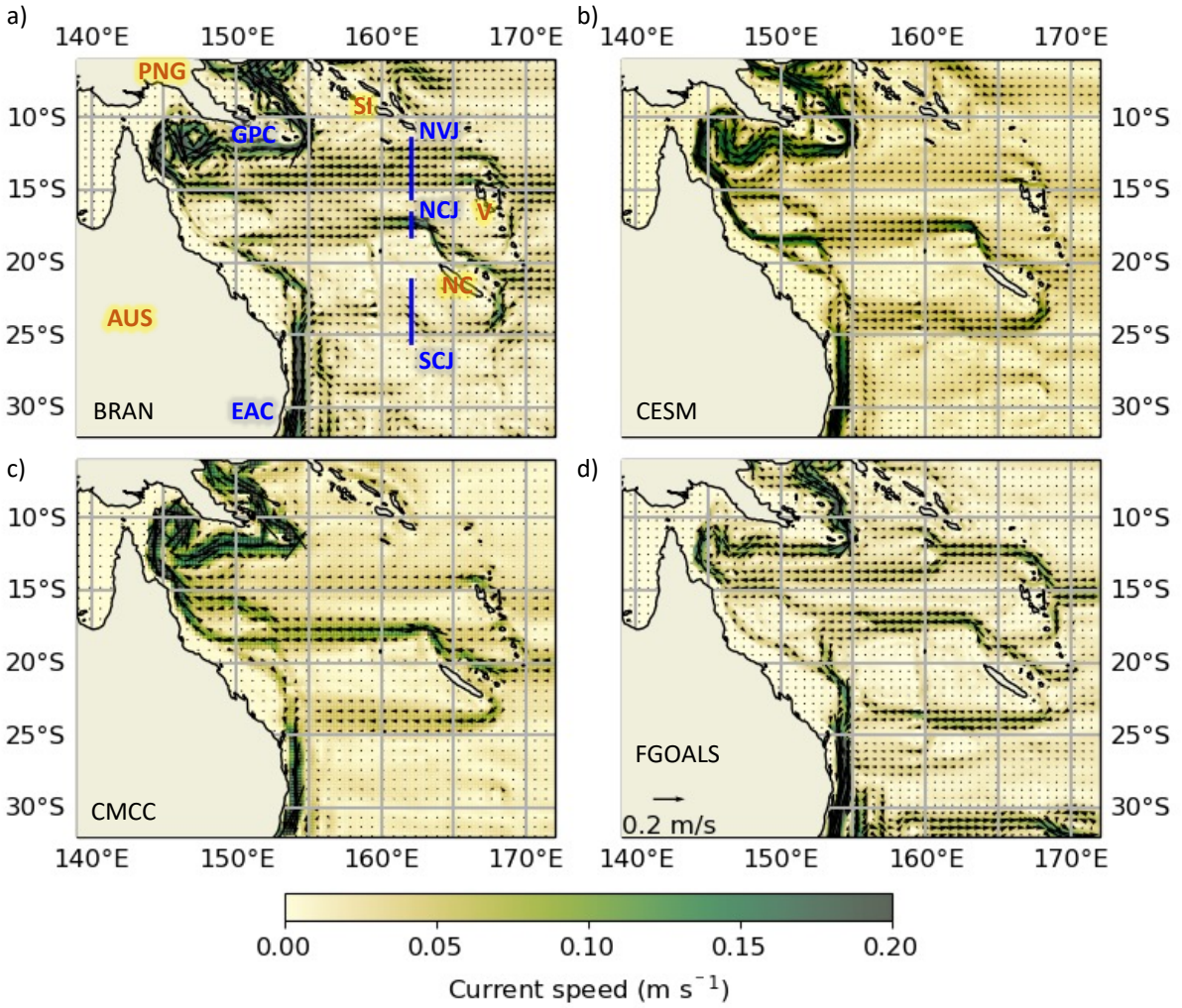

Figure S2. Time (1993 to 2023) and depth (0 – 1000 m) averaged circulation of the Coral Sea. Current vectors, with length scaled with speed, are overlayed on current speed colour maps. a) BRAN2020, with marked islands (orange; NC = New Caledonia, V = Vanuatu, SI = Solomon Islands, PNG = Papua New Guinea and AUS = Australia) and current jets (blue; NVJ = North Vanuatu Jet, NCJ = North Caledonian Jet, SCJ = South Caledonian Jet, GPC = Gulf of Papua Current, EAC = East Australian current). The blue lines show where the jet-specific zonal slices of the currents were taken in the spatial extraction. b) CESM, c) CMCC and d) FGOALS.

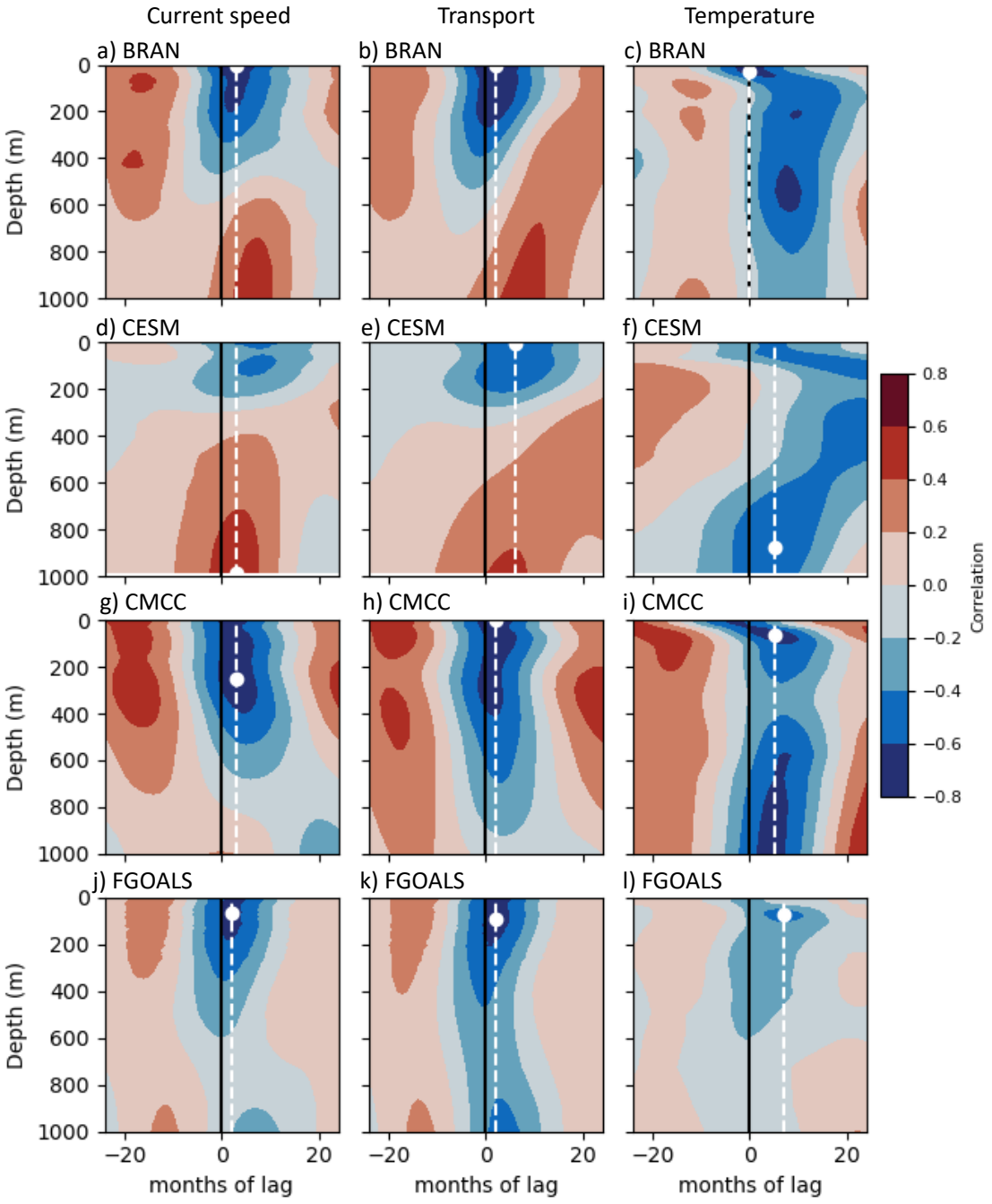

Figure S3. The depth-resolved cross-correlation of NVJ current speed (first column), volume transport (second column) and temperature (third column) interannual anomalies with the Niño 3.4 index. Row 1 = BRAN2020 (a, b, c), row 2 = CESM (d, e, f), row 3 = CMCC (g, h, i) and row 4 = FGOALS (j, k, l). The black lines show zero lag, the white lines indicate the monthly lag corresponding to the greatest absolute value correlation, and the white dots indicate the depth of the greatest correlation.

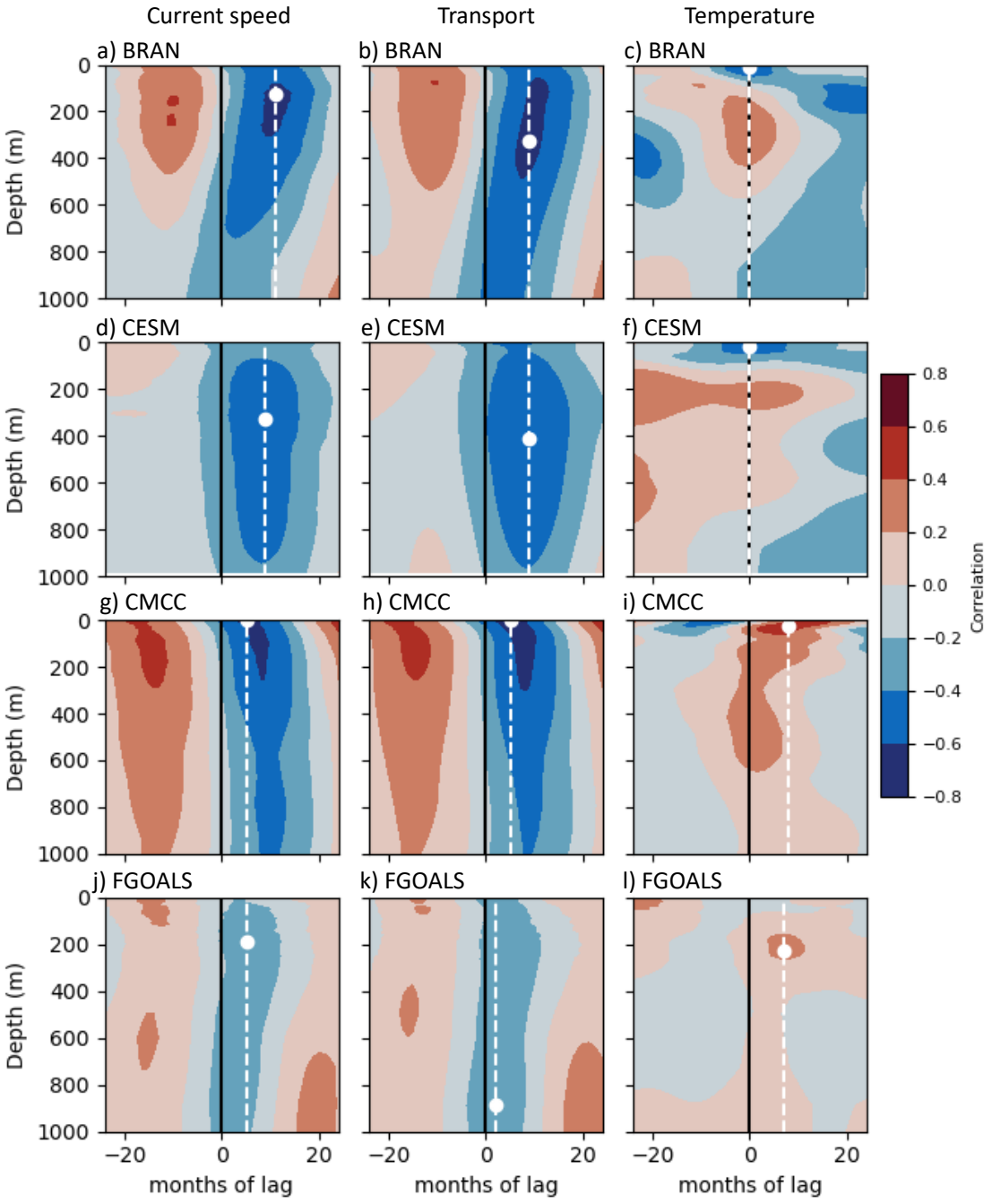

Figure S4. The depth-resolved cross-correlation of NCJ current speed (first column), volume transport (second column) and temperature (third column) interannual anomalies with the Niño 3.4 index. Row 1 = BRAN2020 (a, b, c), row 2 = CESM (d, e, f), row 3 = CMCC (g, h, i) and row 4 = FGOALS (j, k, l). The black lines show zero lag, the white lines indicate the monthly lag corresponding to the greatest absolute value correlation, and the white dots indicate the depth of the greatest correlation.

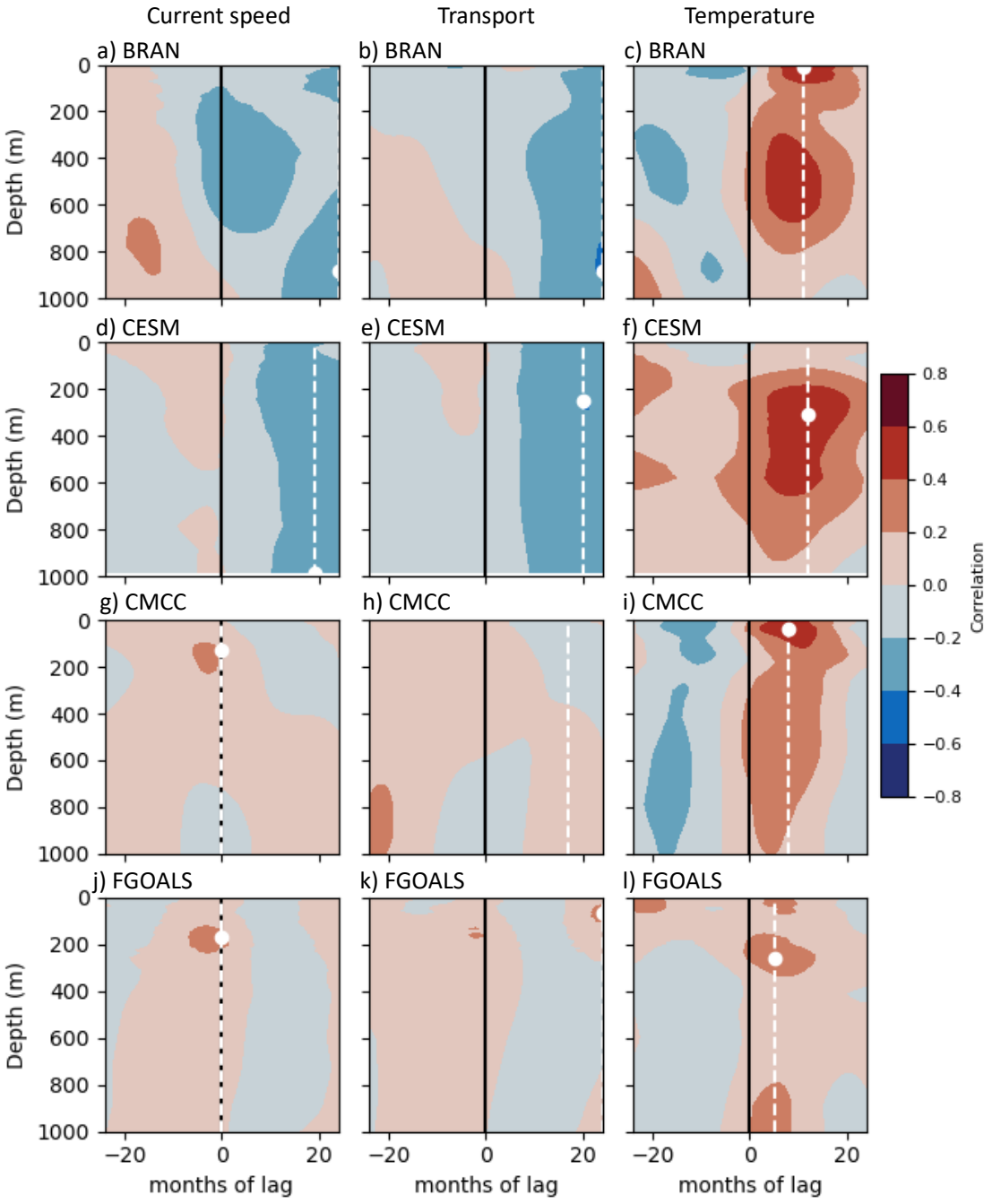

Figure S5. The depth-resolved cross-correlation of the SCJ current speed (first column), volume transport (second column) and temperature (third column) interannual anomalies with the Niño 3.4 index. Row 1 = BRAN2020 (a, b, c), row 2 = CESM (d, e, f), row 3 = CMCC (g, h, i) and row 4 = FGOALS (j, k, l). The black lines show zero lag, the white lines indicate the monthly lag corresponding to the greatest absolute value correlation, and the white dots indicate the depth of the greatest correlation.

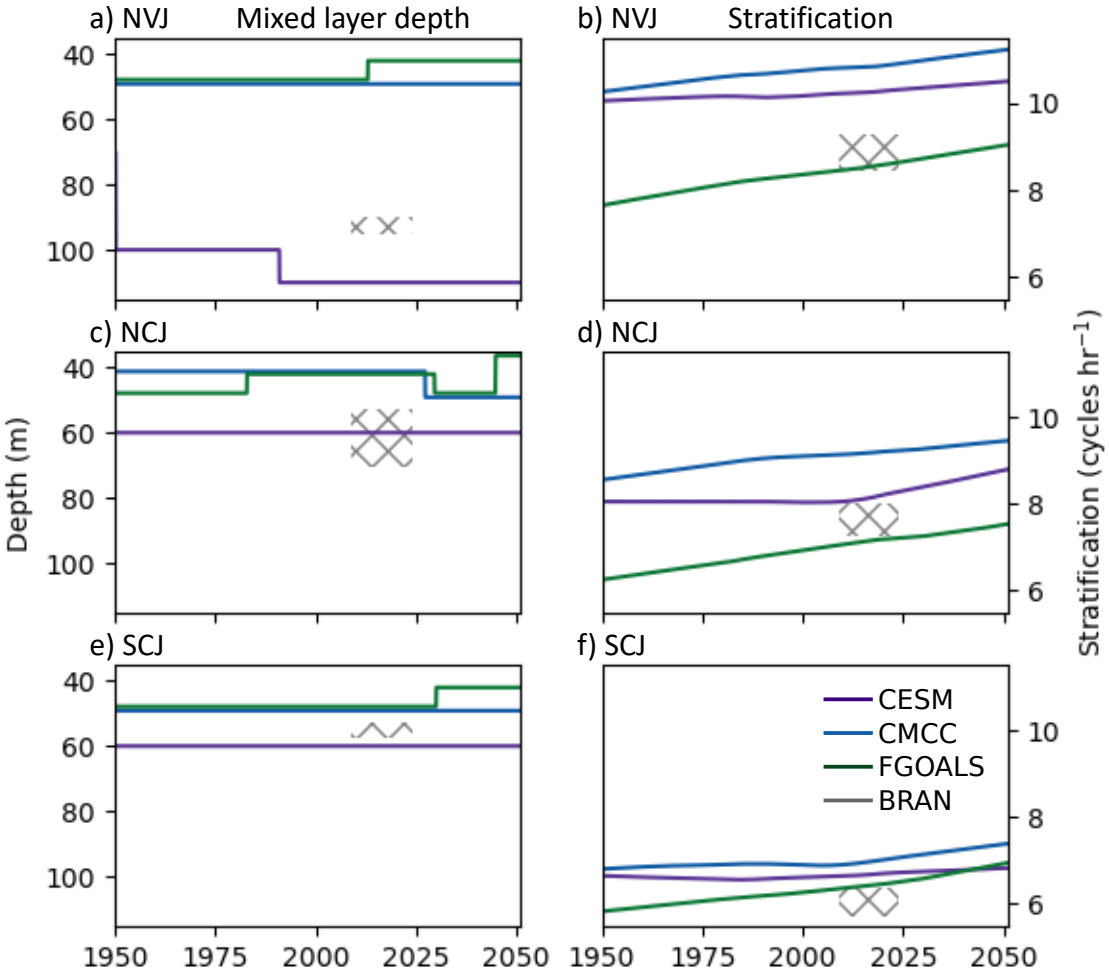

Figure S6. Stratification measures through time, calculated from the trends in temperature and salinity. Mixed layer depth (column 1) and level of stratification (column 2). a, b) NVJ. c, d) NCJ. e, f) SCJ. The grey hatch pattern indicates the range calculated for BRAN2020 in the period from 1993 to 2023.

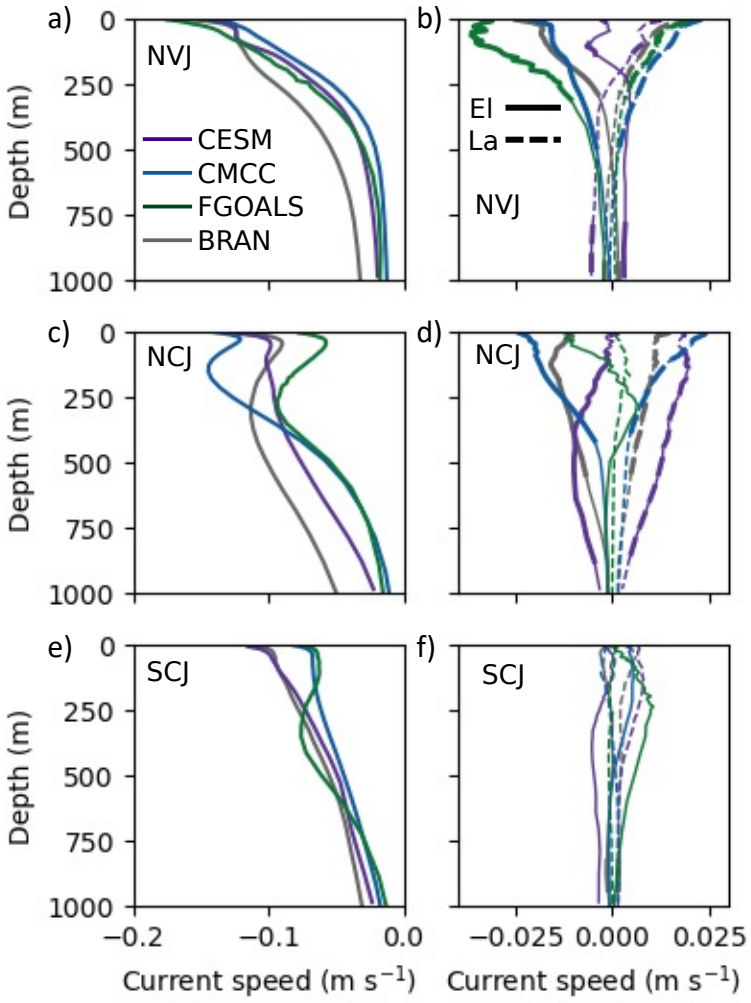

Figure S7. South Equatorial Current jet historical assessment of current speed (1993 - 2023). a) NVJ climatological trend. b) NVJ anomalies associated with El Niño (solid lines) and La Niña (dashed lines) conditions. The anomalies are the averages of instances where Niño 3.4 index > 0.4 for El Niño conditions and < -0.4 for La Niña conditions, with timings offset by the lags corresponding to the greatest correlations identified from the cross-correlation with the Niño 3.4 index (Figure S3 – S5). The lines are bold at depths where the correlation >= 0.4, calculated from the cross-correlation profiles cut at the maximum correlation. c) NCJ climatological trend. d) NCJ El Niño and La Niña anomalies. e) SCJ climatological trend. d) SCJ El Niño and La Niña anomalies.

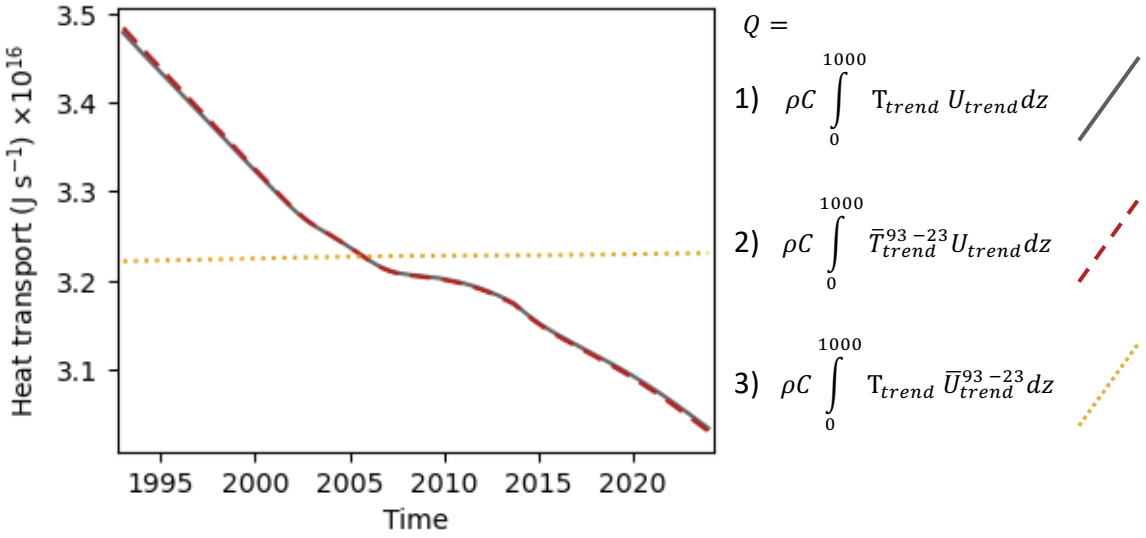

Figure S8. Relative contributions of transport (U) and temperature (T) to heat transport (*Q*). BRAN2020 NVJ 0 – 1000 m heat transport from 1993 to 2023 calculated with: 1) time-varying transport and temperature (solid grey line), 2) time-varying transport and climatological temperature (dashed red line) and 3) climatological transport and time-varying temperature (dotted yellow line). Where heat transport was calculated with time-varying transport and climatological temperature, it closely tracked the control calculation with time-varying transport and time-varying temperature. In contrast, the change in heat transport through time was comparatively small when calculated with climatological transport and time-varying temperature. Thereby, variability in the heat transported by the NVJ was more dependent on variability in transport than temperature.

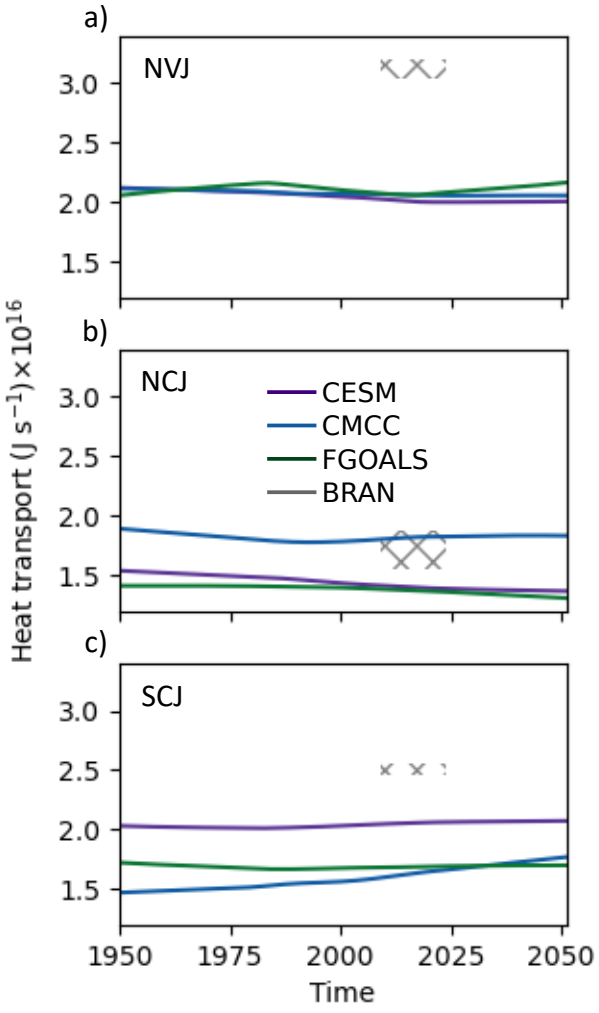

Figure S9. Heat transport trend. a) NVJ, b) NCJ, c) SCJ. The grey hatch pattern indicates the range calculated for BRAN2020 in the period from 1993 to 2023.

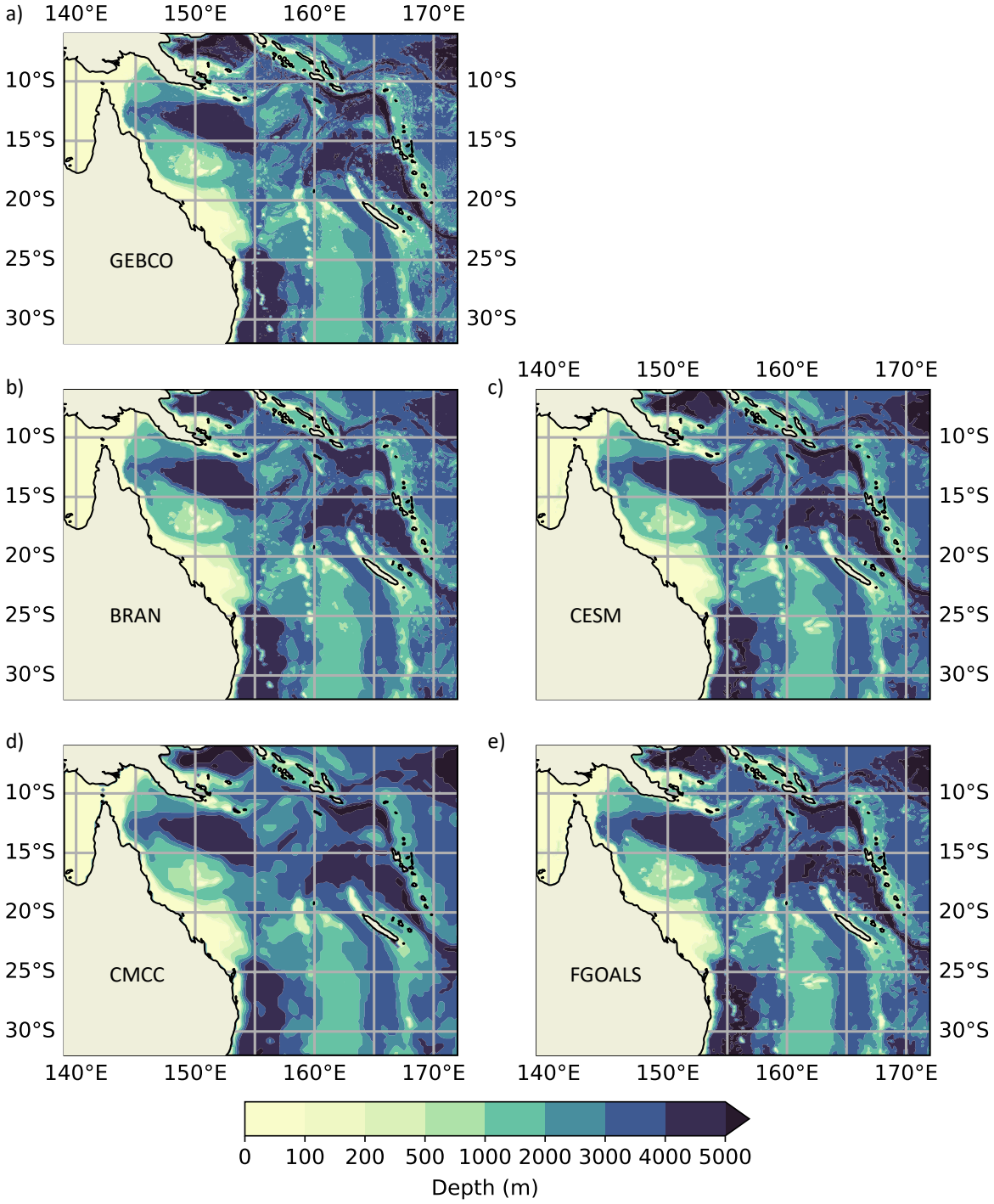

Figure S10. Bathymetry comparison. a) GEBCO 2023, b) BRAN2020, c) CESM, d) CMCC and e) FGOALS.

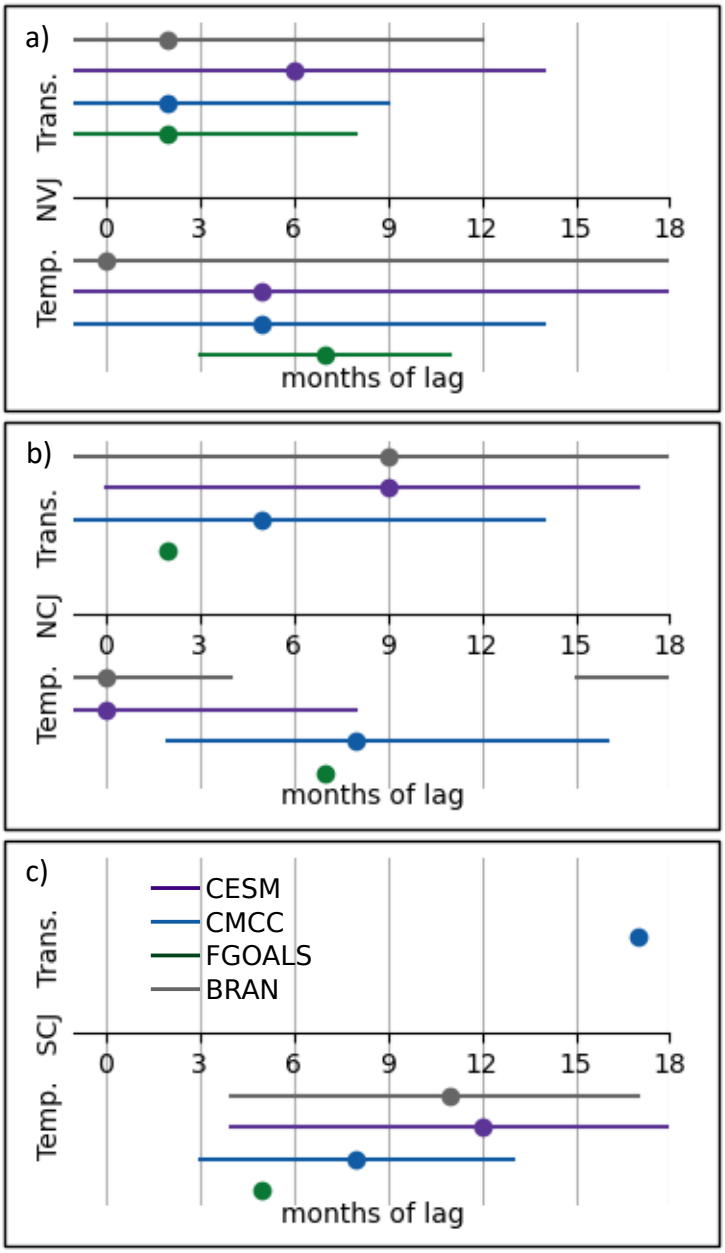

Figure S11. Monthly lag times of correlations between the Niño 3.4 index and transport (Trans.) and temperature (Temp.) interannual anomalies. The lines indicate the lags where there was at least a moderate correlation (|cross-correlation| >= 0.4) at any depth, and the dots indicate the lag of the maximum correlation. a) NVJ, b) NCJ, c) SCJ.

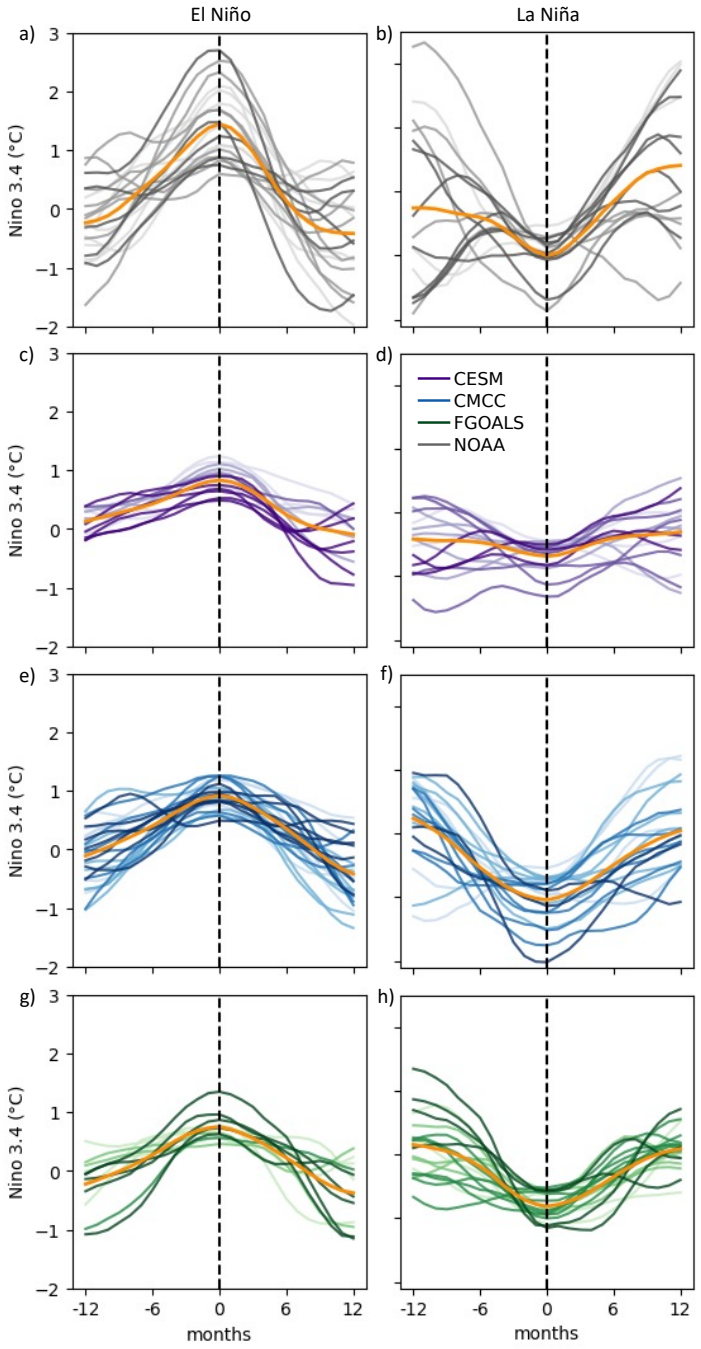

Figure S12. Niño 3.4 anomalies associated with El Niño (first column; Niño 3.4 ≥ 0.4) and La Niña (second column; Niño 3.4 ≤ 0.4) events. The dashed lines indicate the peak Niño 3.4 index associated with the events, and the anomalies 12 months before and after the peak are shown. a, b) Observed. National Oceanographic and Atmospheric Administration (NOAA; https://www.cpc.ncep.noaa.gov/data/indices/). c, d) CESM. e, f) CMCC. g, h) FGOALS. The line shadings correspond to quarter centuries with light to dark successively indicating 1950 to 1974, 1975 to 1999, 2000 to 2024 and 2025 to 2050. The orange lines indicate the averages across events.

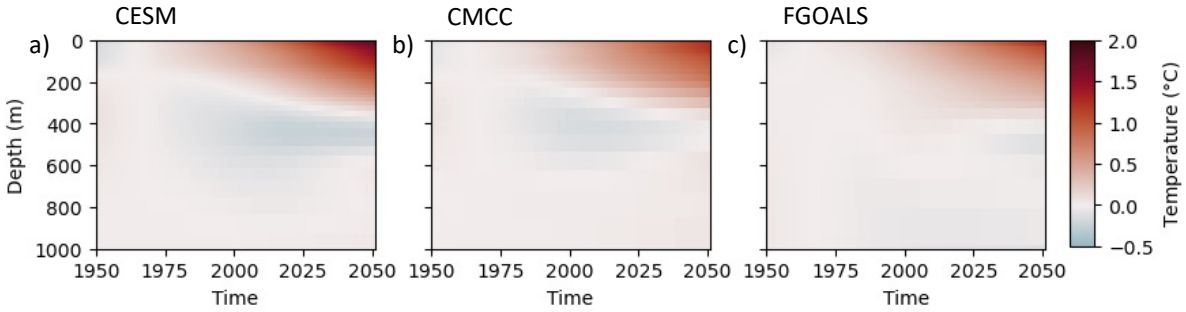

Figure S13. Change in Coral Sea temperature trend (relative to 1950 – 1979) in the HighResMIP models a) CESM, b) CMCC and c) FGOALS.

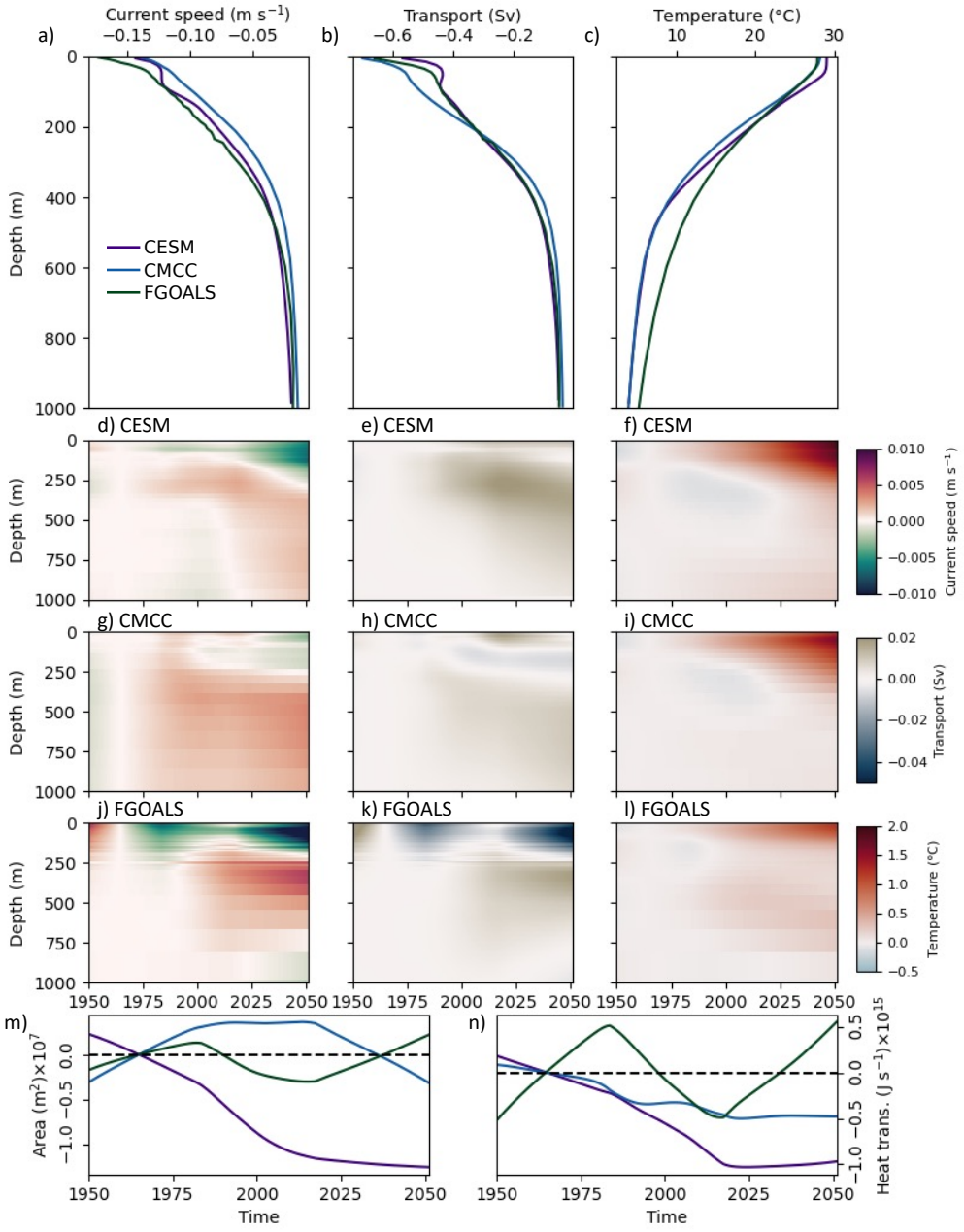

Figure S14. HighResMIP model projected change in the NVJ (relative to 1950 – 1979). Row 1: Trend climatologies of a) current speed b) volume transport and c) temperature. Anomalies from climatologies: d) CESM current speed, e) CESM volume transport, f) CESM temperature, g) CMCC current speed, h) CMCC volume transport, i) CMCC temperature, j) FGOALS current speed, k) FGOALS volume transport, l) FGOALS temperature, m) current area in 0 – 1000 m, n) heat transport in 0 – 1000 m. For visualization, the volume transport has been calculated over 10 m depth bins. For the speed anomalies, positive (red) is a decrease westward and negative (green) is an increase westward. For the transport anomalies, positive (brown) is a decrease westward and negative (blue) is an increase westward.

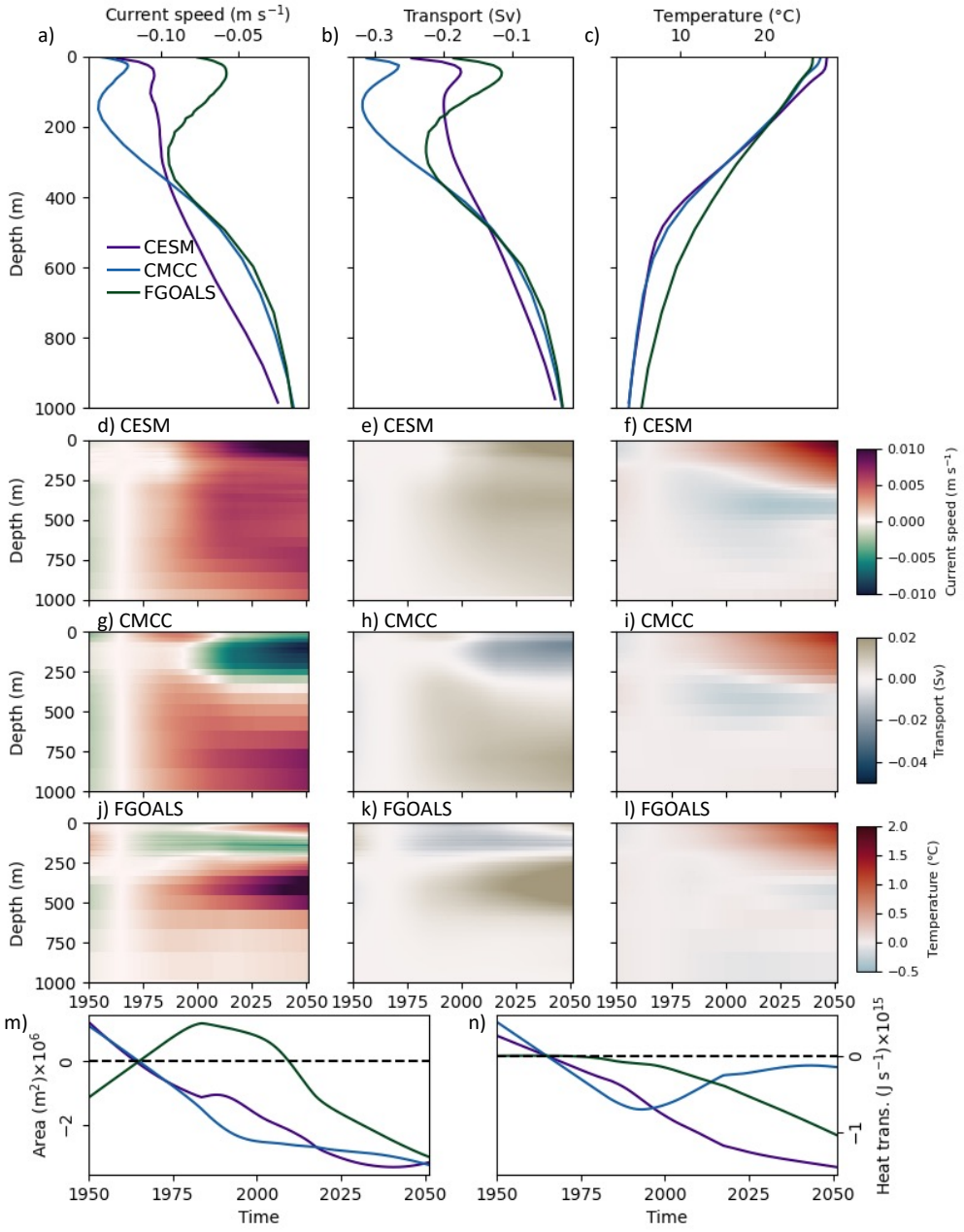

Figure S15. HighResMIP model projected change in the NCJ (relative to 1950 – 1979). Row 1: Trend climatologies of a) current speed b) volume transport and c) temperature. Anomalies from climatologies: d) CESM current speed, e) CESM volume transport, f) CESM temperature, g) CMCC current speed, h) CMCC volume transport, i) CMCC temperature, j) FGOALS current speed, k) FGOALS volume transport, l) FGOALS temperature, m) current area in 0 – 1000 m, n) heat transport in 0 – 1000 m. For visualization, the volume transport has been calculated over 10 m depth bins. For the speed anomalies, positive (red) is a decrease westward and negative (green) is an increase westward. For the transport anomalies, positive (brown) is a decrease westward and negative (blue) is an increase westward.

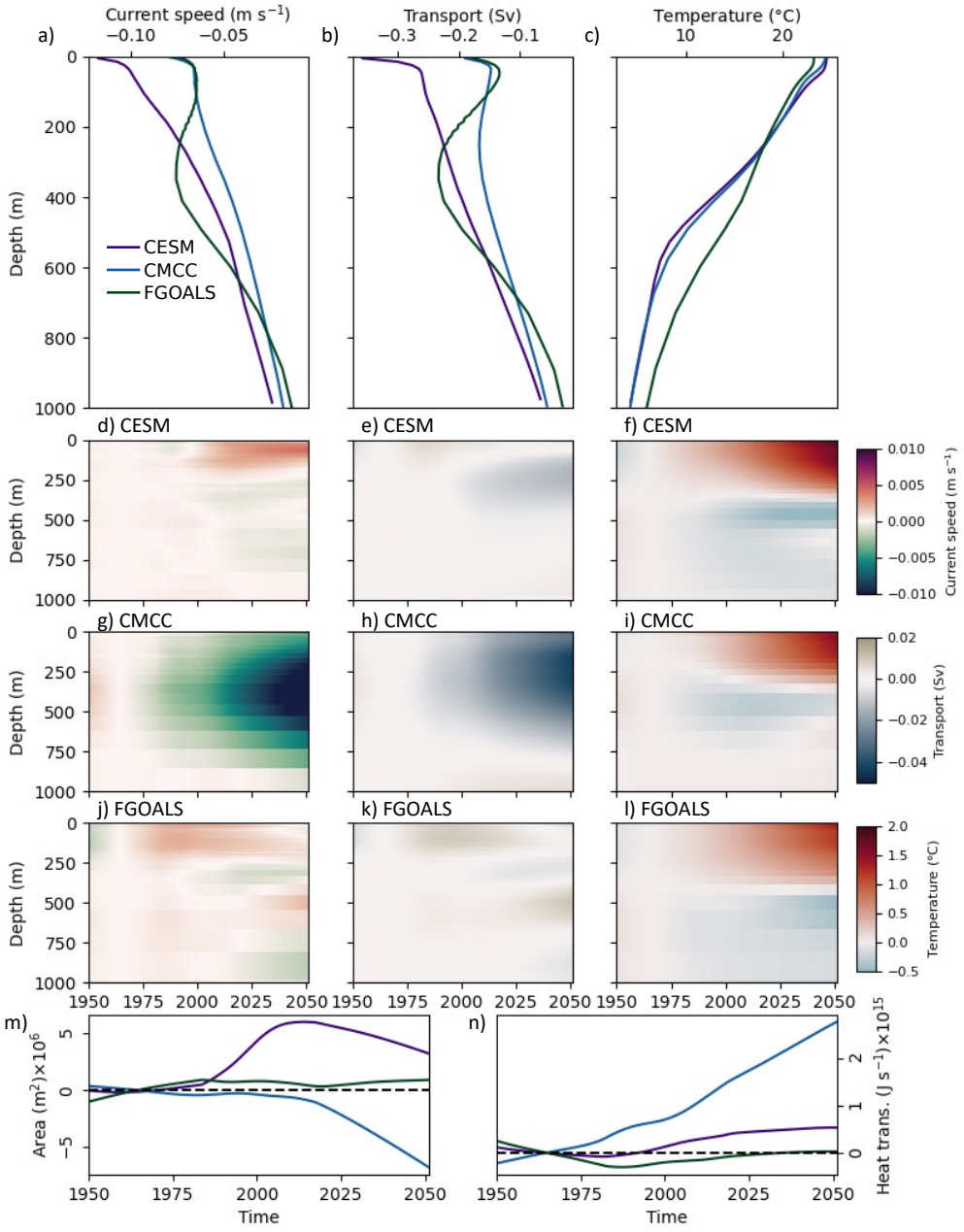

Figure S16. HighResMIP model projected change in the SCJ (relative to 1950 – 1979). Row 1: Trend climatologies of a) current speed b) volume transport and c) temperature. Anomalies from climatologies: d) CESM current speed, e) CESM volume transport, f) CESM temperature, g) CMCC current speed, h) CMCC volume transport, i) CMCC temperature, j) FGOALS current speed, k) FGOALS volume transport, l) FGOALS temperature, m) current area in 0 – 1000 m, n) heat transport in 0 – 1000 m. For visualization, the volume transport has been calculated over 10 m depth bins. For the speed anomalies, positive (red) is a decrease westward and negative (green) is an increase westward. For the transport anomalies, positive (brown) is a decrease westward and negative (blue) is an increase westward.

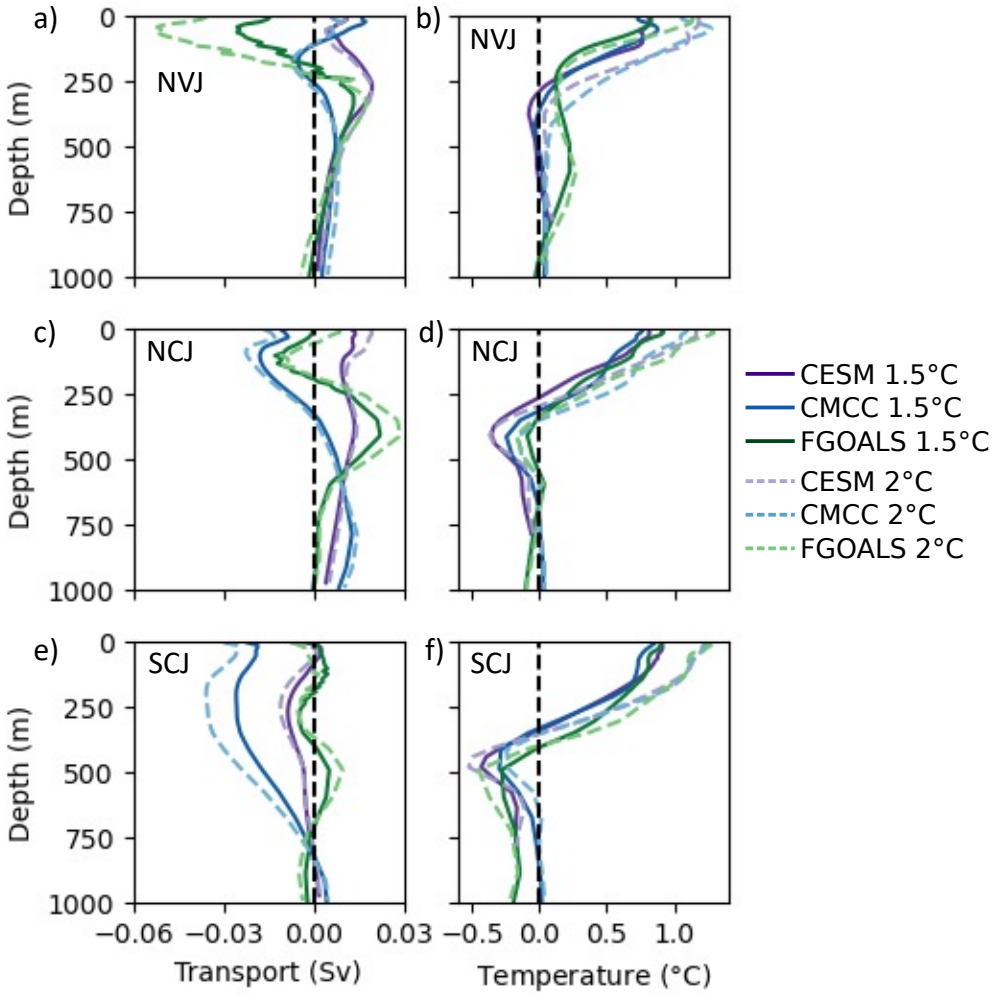

Figure S17. Projected changes in the transport (column 1) and temperature (column 2) trends of the South Equatorial Current jets at 1.5°C (dark, solid lines) and 2°C (light, dashed lines) global warming and relative to 1950 - 1979. Volume transport and temperature anomaly profiles were extracted on dates specific to each HighResMIP model (Table S1). a) NVJ volume transport. b) NVJ temperature. c) NCJ volume transport. d) NCJ temperature. e) SCJ volume transport. f) SCJ temperature. For visualization, the volume transport has been calculated over 10 m depth bins.